A Quantitative Model of Ultraviolet Matrix-assisted Laser Desorption and Ionization

R. Knochenmuss

Author's final revised manuscript.
Published as J. Mass Spectrom., vol. 37, pp. 867-877 (2002)
DOI: 10.1002/jms.349
URL:http://onlinelibrary.wiley.com/doi/10.1002/jms.349/abstract

Abstract

A quantitative model of primary ionization in ultraviolet matrix-assisted laser desorption/ionization (UV-MALDI) is presented. It includes not only photochemical processes such as exciton pooling, but also the effects of the desorption event. The interplay of these two is found to be a crucial aspect of the MALDI process. The desorbing plume is modelled as an adiabatic expansion with entrained clusters. The parameters in the model are defined as much as possible via experiment or by analogy with known effects. The model is applied to the matrix 2,5 dihydroxybenzoic acid, and is found to reproduce the fluence dependence of the fluorescence yield, and key features of the picosecond 2-pulse ion generation efficiency curves. In addition, the model correctly predicts a fluence rather than irradiance threshold, the magnitude of the threshold, the magnitude of the ion yield, laser wavelength effects, plume temperatures, plume expansion velocities, and the spot size effect.

Introduction

It is currently considered highly likely that ionization in MALDI (Matrix Assisted Laser Desorption/Ionization) is the result of two major processes.(1, 2) During or shortly after the laser pulse, primary ions are generated. In the ensuing desorption plume expansion, ion-molecule reactions convert the primary ions to the most favorable secondary products. These are finally observed at the detector.(1, 3) Evidence is accumulating that the plume generally approaches equilibrium, allowing secondary processes, and hence the mass spectrum, to be well understood in terms of gas-phase thermodynamics.(1, 3)

On the other hand, in spite of significant interest, the primary ionization processes in MALDI have remained more puzzling.(2, 4) Among the reasons for this were the paucity of mechanistically unambiguous experimental data as well as the inability of qualitative models to provide quantitatively testable predictions. The former difficulty has recently been recognized as a consequence of secondary processes, which mask the primary events.(1) The second problem has followed from the first, as investigators have not had a sufficient base on which to build detailed models.

Recognition of the two-step nature of MALDI ionization as well as recent experimental studies have made it possible to advance the theory of MALDI. We present here a model for primary UV MALDI ionization in one matrix, with no analyte. It yields detailed and quantitative predictions that are in good to excellent agreement with experiment. While questions remain, it provides a strong working hypothesis for further study.

Important to the development of the model is the choice and use of experimental data to test and constrain it. A remarkable and useful MALDI phenomenon is the 2-pulse effect.(5-7) MALDI is a nonlinear process, more dependent on fluence than on peak power.(8-14) As a result there is typically a "threshold" fluence above which signal first becomes signficant. In the 2-pulse effect, time delayed sub-threshold pulses, which individually give negligible signal, together give a strong mass spectrum.

The 2-pulse effect has been taken as one of several indicators of pooling process in ion generation.(5) Qualitatively, pooling as a MALDI mechanism goes back to early studies.(15) More detailed evidence for it was obtained later(5) and it began to be taken more seriously after it was demonstrated that matrix ionization potentials generally lie too high for 2-photon ionization with the usual lasers.(2, 16, 17)

Pooling was included in our early quantitative model.(16) That model was built upon the rate equation picture proposed by Allwood and Dyer.(18, 19) It was shown that even for quite moderate pooling rate constants, it could be an efficient process. Direct experimental evidence for pooling is difficult to obtain, but the fluence dependence of fluorescence from some MALDI matrices seems to point strongly in this direction.(20) Those results were fit by the authors with a simplified model including a pooling step.

The 2-pulse effect and fluence dependence of the fluorescence yield are the most important data used to constrain the present model. With no further adjustement, several other experimentally known aspects of MALDI are correctly predicted.

Model

The rate equation approach(16, 18, 19) treats the MALDI sample as a continuous medium for which a microscopic description of molecular-scale events is not necessary, and for which temperature is well defined. These approximations appear to work well as applied here, but may in future need to be refined in light of molecular dynamics simulations which can be used to investigate non-equilibrium effects.(21-24)

The model includes rate equations for: the matrix ground electronic state (S_0), the first excited singlet state (S_1), a higher excited singlet state (S_n, at twice the photon energy, but below the ionization potential), the ion state, and the matrix internal energy (i.e. local temperature). No triplet states are considered, as no evidence for significant intersystem crossing was found in spectroscopic studies of DHB.(16) Pooling is accounted for by non-linear terms involving the product of two excited states. No analyte is included at present, only the matrix is modelled.

The differential equations to be integrated are (see also Table 1 and Figure 1):

$$\frac{\mathrm{d}[S_0]}{\mathrm{d}t} = -I(t)\sigma_{01}(\lambda)[S_0] + \frac{[S_1]}{\tau_1} + I(t)(\sigma_{01}(\lambda)/5)[S_1] + Dk_{11}[S_1]^2 + Dk_{1n}[S_1][S_n] + k_{I0}[\mathrm{Ions}]$$

$$\frac{\mathrm{d}[S_1]}{\mathrm{d}t} = I(t)\sigma_{01}(\lambda)[S_0] - \frac{[S_1]}{\tau_1} - I(t)(\sigma_{01}(\lambda)/5)[S_1] - I(t)\sigma_{1n}(\lambda)[S_1] + k_{n1}[S_n] - 2Dk_{11}[S_1]^2 - Dk_{1n}[S_1][S_n]$$

$$\frac{\mathrm{d}[S_n]}{\mathrm{d}t} = I(t)\sigma_{1n}(\lambda)[S_1] - k_{n1}[S_n] - k_{\mathrm{therm}}[S_n] + Dk_{11}[S_1]^2 - Dk_{1n}[S_1][S_n]$$

$$\frac{\mathrm{d}[\mathrm{Ions}]}{\mathrm{d}t} = k_{\mathrm{therm}}[S_n] + Dk_{1n}[S_1][S_n] - Dk_{I0}[\mathrm{Ions}]$$

$$\frac{\mathrm{d}E}{\mathrm{d}t} = I(t)\sigma_{01}(\lambda)[S_0][h\nu - E(S_1)] + \frac{1}{\tau_1}\{[S_1]E(S_1)(1 - \Phi(S_1)) + k_{n1}[S_n][E(S_n) - E(S_1)]\} + Dk_{1n}[S_1][S_n][E(S_1) + E(S_n) - IP] + Dk_{I0}[\mathrm{Ions}]IP$$

$$\mathrm{Temperature} = E/(kf)$$

$$k_{\mathrm{therm}} = 9 \times 10^{15} \mathrm{e}^{[E(S_1)-IP]/kT}$$

I(t) is the laser intensity, $\sigma(\mathrm{I})$ an absorption cross section at the laser wavelength, $E(X)$ the energy of state X, f the internal degrees of freedom and k Boltzmann's constant. D describes the range of the pooling process, here held at 6 for the number of nearest neighbors.(16) The parameters t_1 (and therefore the quantum efficiency, $\Phi(S_1)$) k_{11}, k_{1n}, k_{I0} are time dependent after desorption starts, as described below. The thermal ionization rate expression is from Ref. (18, 19). Excess energy of ionization processes above the IP is assumed to be converted to heat. The ion recombination energy is approximated to be equal to the ionization potential, IP.

Pooling Processes

It is important to note that the S_1 + S_1 pooling process here leads to the S_n state, and not to ions, as illustrated in Fig. 1. The ionization potential lies too high for generation of DHB^+ (or $(DHB)_n^+$) at twice the S_1 energy (6.93 eV).(16, 17) From the S_n, the S_1 is relatively quickly regenerated, with associated heating of the sample. This is fundamentally different from the model of Ref.(20), where S_1 + S_1 pooling was assumed to lead to an unspecified sink state (possibly ions or a triplet), and therefore removed from the futher progress of the simulation. Although the proton disproportionation reaction of DHB is known to be energetically accessible at twice the S_1 energy (2DHB → $DHBH^+$ + $(DHB\text{-}H)^-$ ΔG=5.25 eV(25)), it was found in simulations that such a process gives unreasonable results, producing an excessive population of such ions (up to tens of percent). A more accurate model would include a branching ratio for S_1 + S_1 pooling products, some ionizing via disproportionation and others creating an S_n / S_0 pair. In addition, autoionization via proton disproportionation of the S_n with a neighboring S_0 would need to be included. The

necessary parameters for these processes were considered to be too difficult to estimate with available data, so only the $S_1 + S_1 \rightarrow S_n + S_0$ process was included.

Stimulated Emission

Stimulated emission from the S_1 state is included, with a cross section 1/5 that for S_0 to S_1 pumping. This very probably a considerable overestimate since the spectral overlap of the laser with the fluorescence of DHB is much smaller than the overlap with the absorption band. However, the approximation is retained due to the high peak powers of picosecond pulses which will be modelled. It has the effect of reducing the efficiency of pooling processes by depleting the S_1 state, and is therefore a conservative approximation.

Laser Pulse Propagation

The laser pulse is attenuated as it propagates into the sample. The depth-dependent ion yield is not a linear function of the laser intensity, making it necessary to sum individually calculated contributions from many sample layers below the surface. For each layer the laser pulse is attenuated by the previously calculated overlying layers. The layers are sliced so as to achieve equal absolute attenuation in each layer. This has the desirable effect of using thinner layers near the surface where intensities are highest and non-linear effects largest. In addition, the laser attenuation is time-dependent due to the varying concentrations of S_0, S_1 and S_n states. The pulse was therefore numerically propagated into the sample for each time point in the calculation, using concentrations in the previous layer to calculate the new laser profile.

Molecular Beam Plume Model

Desorption is modelled by adding two features to the model. When the temperature reaches the experimentally determined sublimation temperature (450 K for DHB)(26), the sample is presumed to begin expanding into the vacuum. This is modelled as an adiabtic, isentropic supersonic expansion.(27) The critical parameter describing such an expansion is the ratio of the downstream distance to the diameter of the source, typically denoted as x/d. In this case d is given by the laser spot size. After the sublimation temperature is reached, the sample begins to move into the vacuum, its speed increasing and its density decreasing as predicted for a supersonic expansion:

$$X = x/d$$

$$M = c - a\mathrm{e}^{-AX} - b\mathrm{e}^{-BX}$$

$$\mathrm{v}_{\mathrm{sound}} = \sqrt{\frac{\gamma RT}{(MW)}}$$

$$\mathrm{velocity}(X) = M\mathrm{v}_{\mathrm{sound}}$$

$$\gamma = \mathrm{C_P}/\mathrm{C_V} = 1.05$$

$$\frac{\mathrm{P}}{\mathrm{P}_0} = \left(1 + \frac{\gamma}{\gamma - 1}M^2\right)^{-\gamma/\gamma - 1}$$

Where d is the laser spot diameter from which the plume is emitted, x is the downstream distance from the desorption surface, M is the Mach number of the expansion, vsound is the ideal gas speed of sound, for molecules of molecular weight MW, and P is the pressure. The constants a, b, c, A and B were obtained from a fit to the expressions given in Table 2.1 of Miller.(27) The biexponential fit was used in order to extrapolate to small x/d values. The constants used were: c=6.982, a=1.489, b=3.036, A=1.5, B=0.4282. The value of A from the fit was 0.2. However, this leads to a comparatively slow acceleration of the plume, which is clearly not consistent with experiment or molecular dynamics simulations.(21-24, 28) To steepen the expansion curve, A was increased. This has a relatively small effect on the end velocities. As will be seen below, even with this modification, the expansion of the plume is probably still modelled as accelerating somewhat too slowly.

Effect of the Plume on Model Parameters

The plume expansion must have an effect on pooling processes since they require molecules to be in contact. The pooling rates are therefore scaled downward after the start of desorption, by the calculated plume pressure (P/Po). In addition the S_1 lifetime of free molecules is affected, since condensed phase or collisional quenching processes become less important. For the matrix considered here, 2,5 dihydroxybenzoic acid (DHB), the fluorescence lifetime in the solid is near 1 ns,(20) while we have measured 30±2 ns in the gas phase. In the model, the lifetime is scaled by 1/(P/Po), but since the time period relevant for ionization is short compared to the full plume expansion (ns vs. ms), the lifetime was only allowed to increase a small amount from the solid lifetime, to 3 ns. It should be noted that knowlege of the true gas phase lifetime is important even if it assumed that this lifetime is not reached in the simulated plume. The ratio of the instantaneous lifetime to the limiting lifetime

gives the quantum efficiency of fluorescence, and hence the amount of S_1 energy that is converted to heat by internal conversion, or emitted as fluorescence.

The very limited ability of ions to escape from the solid was included in the model by adding a term to the differential equations for recombination. Recombination obviously becomes slower as plume expands and the relevant species are physically separated. This was taken into account by scaling the recombination rate downward with P/Po.

Clusters in MALDI Plumes

It has been experimentally(29, 30) and theoretically(21-24) shown that a substantial fraction of the ablated MALDI sample is ejected in the form of chunks or clusters. The molecular dynamics simulations suggest that the fraction of "solid" material is around 1/6 over a range of laser fluences. This is very important for obtaining an accurate simulation since the properties of the chunks are more like those of the solid matrix and not of free molecules. In particular the fluorescence lifetime is low and ions formed within the solid will not escape to be detected at the correct m/z ratio. This effect is easily modelled. Two simulations are perfomed, one with and one without plume expansion. The former represents that part of the sample which is ejected as molecules (15%) and the latter represents the solid chunks (85%). The results for the two are added together with these weighting factors to give the final result.

Summary of the Method

At this point is perhaps useful to step back from the details described above and to summarize the logic of the algorithm used:

```
Start loop over fluences (or 2-pulse delays)
   Define laser pulse vs. time for top layer
   Start loop over depth layers
      Calculate next layer thickness (constant attenuation/layer)
      Calculate laser pulse for next layer (based on attenuation vs. time
                                          for the preceding layer)
      Integrate differential equations over time:
         Calculate derivatives for all species and internal energy
         If temperature >= sublimation temperature
            Calculate plume expansion since time when Tsubl reached
            Scale parameters by reduced pressure, P/P0
         Endif
      End integration loop over time steps
      Check quality of integration
      Sum fluorescence (=S1(t)F(t)) over time for this layer
   End loop over layers
   Sum results over all layers, weighted by layer thickenesses
End loop over fluences (or 2-pulse delays)
Normalize fluoresence yield to fluences
```

If clusters are included, the above procedure is repeated, but without any plume expansion. The results with and without expansion are summed with weight factors corresponding to the mole fractions of free and cluster matrix.

Parameters used

Only one matrix is modelled, 2,5 dihydroxybenzoic acid (DHB), since the necessary data is not available for others. Parameters used in the simulation are listed in Table 1. Those parameters not directly available from experiment are discussed below.

Radiative Processes

The $S_1 \rightarrow S_n$ absorption coefficient was conservatively set to be 1/5 of the $S_0 \rightarrow S_0$ absorption coefficient, from spectroscopic experience with DHB in molecular beams. Multi-photon effects at the $S_0 \rightarrow S_1$ absorption wavelength were sought by increasing the laser pulse energy dramatically above that needed for good fluorescence intensity, but none could be observed. This included fluorescence quenching, new fluorescence bands or multi-photon ionization. In view of the lack of such effects, 1/5 of the $S_0 \rightarrow S_0$ absorption coefficient is almost certainly too high. In the present context this is considered conservative since it emphasizes single center processes, at the expense of pooling.

Non-radiative S_n Decay

The high $S_1 \leftarrow S_n$ decay rate reflects Kasha's rule that fluoresence is not observed from higher excited states due to rapid internal conversion. The rate selected is typical or slightly below average by comparison with other aromatics.(31) $S_1 + S_1$ pooling and this decay path work against each other to a certain extent. This does not make them mutually dependent, since the effects are not equivalent, and the rate constants differ by an order of magnitude.

Ion Recombination

From ultrafast studies on ion/trapped electron pairs (polarons) the time constant for recombination is expected to be on the order of a few picoseconds.(32) The rate selected is typical for such processes, neither very high nor very low.

$S_n + S_n$ Pooling

Pooling of two Sn excitations to yield ions can also be included in the model, but S_n populations were typically sufficiently low that this process had no effect on the results, for rate constants in any reasonable range. It was therefore neglected in the results shown here.

Thermal Ionization from S_n

The thermal ionization expression of Refs. (18, 19) was included, but the temperatures reached were too low for this to make a significant contribution to the ion yield. This is in strong contrast to the conclusions of those studies where very high temperatures were calculated. Such temperatures would be inconsistent with survival of fragile biomolecules in the plume, and are not in agreement with measured temperatures, as noted below.

Numerical Integration

The rate equations were numerically integrated using double precision 5th order Runge-Kutta methods, as included in the Igor data analysis package (WaveMetrics Inc., Lake Oswego, OR, USA). The number of time points was increased until no further change in the result was observed. A large number of time steps was particularly important when using short laser pulses. The depth integration was carried out until the laser was attenuated to <5% of its initial value. The number of depth slices was at least 35.

Results and Discussion

Figure 2 shows simulation results for a nanosecond pulse. Apparent is the effect of desorption on ion generation. The ion concentration only becomes significant after desorption has begun. Ions are formed in the short time during which both S_1 and S_n populations are significant, and the desorption has started. The asymmetry of the S_1 population is also quite pronounced, due to the lifetime increase during desorption.

Fluence Dependence of the Fluorescence Yield

An important consequence of the large cluster fraction in the plume is that the fluorescence yield is determined mostly by the properties of the solid matrix. The small amount of free matrix with a higher S_1 lifetime and quantum yield is overshadowed by the cluster fraction. As a result, it was possible to first estimate the $S_1 + S_1$ pooling rate using the fluorescence data, while setting the parameters related to ion formation or decay to zero. This gave the order of magnitude for the $S_1 + S_1$ pooling rate. This initial estimate was then increased somewhat as the ionization processes were added to fit both the 2-pulse and fluorescence data together.

The ionization-related parameters were initially set to the expected orders of magnitude noted in the model discussion above. Only the $S_1 + S_n$ rate was initially completely unknown, and it was simply selected to be one order of magnitude higher than the $S_1 + S1$ process, because the total energy involved is substantially greater. It is important to note that using physically reasonable initial estimates gave sufficiently good results that only manual adjustment was needed to achieve agreement with all the data. No formal fitting procedure was used.

Figures 3 shows the simulated results for the nanosecond fluence-dependent fluorescence yield, the agreement with the data(20) is excellent in both the high and low fluence ranges. The data at the lowest few fluences is believed to be too high, since it was scaled in the belief that the low fluence limit had been reached.(20) The simulations show that this was probably not quite the case.

Fluorescence yield is the simpler experiment to model, since higher excited states and ionization processes are relatively unimportant. However, the effect of the plume is not negligible. Without the free molecules and their higher quantum yield, the calculated curve would fall too low at the higher fluences. Instead, this deficit is nicely compensated by the free molecules. (At lower fluences little or no material is desorbed, the sample remains solid.) Within the present model for the $S_1 + S_1$ pooling process, the plume is found to be essential for a good fit to this data.

Figure 4a shows how the fluorescence yield depends on some model parameters. Changing the limiting S_1 plume lifetime to 10 ns has a rather large effect at fluences above the desorption threshold. Note that this is still a factor of 3 below the true free molecule lifetime of 30 ns. The overall curve takes on more structure than experimentally observed, this part of the model is well constrained by the fluorescence data.

In contrast, doubling the $S_1 + S_n$ pooling rate has a very minor effect on fluorescence yield curve, as seen in Fig. 4b. Somewhat more S_1 population is lost to ions than before, but this causes only a slight decrease in the simulated results below the experimental data. As will be seen below, however, this has a large effect on the simulation of the two pulse data. Figs. 4a and b illustrate the complementarity of fluorescence and ionization data in constraining different parts of the model in a quasi-independent fashion.

Time Delayed Picosecond 2-pulse Ion Yields

After fluorescence was used to estimate some parameters, it was possible to move on to ion formation, and model the 2-pulse experiment by adjusting the pooling and recombination parameters. An example simulation is shown in Fig. 5. Apparent is the negligible ion yield from the first (sub-threshold) pulse, but the substantial yield of the second, equally weak, pulse. The model thus correctly predicts the existence of a threshold fluence and a 2-pulse effect. The 2-pulse effect appears when the first pulse becomes strong enough to begin desorption but liberates no ions. The expanding plume is then "taken advantage of" by the second pulse to efficiently yield ions.

As Figure 6 shows, the model also reproduces the remarkable shape of the experimental 2-pulse curve(7) in a semi-quantitative manner. The initial peak is rapidly followed by a narrow valley, then a broad peak, with a gradual decay afterwards. (The experimental t=0 peak is presumed to be a result of higher order processes not modelled here.) The main differences are in the smaller modulation of the ion signal than experimentally observed, and the longer time scales. The experimental extrema appear sooner than simulated (minimum: 0.2 vs. 0.5 ns, Fig 6b; maximum: 2 vs. 3 ns, Fig. 6a). It should be noted that recent 2-pulse experiments in our laboratory with carefully purified DHB have shown a delayed maximum at 3 rather than 2 ns. The position of the extrema is also very dependent on the plume expansion time scales, suggesting that the molecular beam approximation used here

underestimates the expansion rate. In particular, it is probably more suddenly accelerated than simulated here. This is expected as a result of the sudden heating of the sample. It will expand with sound velocity (for organic liquids >1000 m/s, for solids up to several 1000 m/s) and throw off the outer sample layer at similar speeds.

An interesting further prediction of the model is that a delayed maximum persists also for fluences individually somewhat above threshold. This arises because the laser intensity for some sub-surface layers is again in the range needed for the effect. This has not yet been experimentally investigated and will be a useful further test.

The fluence dependence of the 2-pulse delay curves is shown in Fig. 7. At low fluences, desorption is induced only by the second pulse, leading to a nearly flat curve with increasing delay. At higher fluences desorption occurs after the first pulse, but before the second. This gives rise to the characteristic double maximum shape of the curve. As the time for the start of desorption moves forward in time with increasing fluence, the positions of the minimum and second maximum of the curves also move to shorter times.

Figure 8 shows the dependence of the 2-pulse delay curves on some model parameters. Curve (a) is calculated with the standard parameter set. Curve (b) shows the effect of a significantly longer limiting S_1 state lifetime, 10 ns instead of 3. This increases the ion yield slightly, and shifts the second maximum a small amount to longer times. The effect is not dramatic in either respect, in contrast to the large effect on the fluorescence yield curves. Curve (c) adds direct photoionization from the S_n (cross section same as $S_0 \rightarrow S_1$) to show the effects of another possible ionization pathway. The positions of the extrema are shifted slightly, and the long-time decay is somewhat faster, but differences compared to the standard parameters are minor. Curve (d) shows the effect of a higher $S_1 + S_n$ rate ($3X10^{11}$ s^{-1} instead of $1.5X10^{11}$ s^{-1}). This is the main ion generation route, and the rate has a correspondingly significant effect.

Part (e) of Fig. 8 shows a simulation without plume expansion, but with pooling. Recombination has been turned off to approximate ionization when the expansion has no effect. This result is particularly interesting because it shows that the plume is extremely important both for the shape of the two pulse curve, and for the magnitude of the ion yield. The rapid decrease from a t=0 maximum is clearly inconsistent with the data, and the ion yield is several orders of magnitude too low. This appears to be strong further evidence for the correctness of the present model.

Threshold Ion Generation Fluences and Laser Wavelength Effects

The threshold fluences predicted by the model correspond remarkably well with the data. As seen in Fig. 9 the threshold for both 30 ps and 4 ns 355 nm pulses is 14-15 mJ/cm^2, the thresholds found in Ref. (7) were 10-20 mJ/cm^2. In accordance with experiment, the threshold is the same for both short and long pulses, there is no peak-power (irradiance) effect. This is because the threshold is largely a matter of desorption, and not, as might be intuitively expected, ion genereration efficiency. The heating of the sample to the desorption temperature is determined mostly by the conversion of S_1 excitations to heat, and the time scale is therefore that of the S_1 state. As long as some S_1 population remains or is generated after desorption starts, ions will be released.

That desorption limits the fluence threshold is also illustrated by the results for 337 nm excitation (N_2 laser) in Fig. 9. The absorption cross section at this wavelength is about 7 times larger than at 355 nm, and the photon energy is further above the minimum S_1 energy. These factors lead to a more rapid heating of surface layers, and hence liberation of ions at lower fluences. As is known experimentally,(33, 34) the model shows that MALDI is more efficient if the matrix more strongly absorbs the laser.

Slower laser pulses generate lower instantaneous S_1 populations and hence fewer ions at a given fluence. The 4 ns pulse yields fewer ions above threshold than the 30 ps pulse. The increased efficiency of the short pulse is, however, clearly far less than the difference in peak powers (2 orders of magnitude). Even above threshold UV-MALDI is correctly predicted by the model to be much more fluence- than irradiance-dependent.

The ion signal from the surface layers rises with a moderate 2.5 (ns, 355 nm; 1.7, 337 nm) or 2.8 (ps, 355 nm) power of the fluence. This corresponds, in a certain sense, to the "true" fluence dependence of MALDI, where desorption is only relevant for the threshold and has little effect thereafter. When the depth integration is also carried out, it is mainly the exponential prefactor that changes. The two 355 nm curves then rise with the 2.5^{th} power of the fluence, the 337 nm curve with the 1.8^{th} power.

These exponents are less than the 6th power dependence found by Dreisewerd, et al. for DHB.(13) However, it must be recalled that the neutral desorbed density was also found to have an even steeper fluence dependence (10th power). Such a drastic fluence dependence of the desorbed quantity is not a feature of the present model since it cannot take directly into account the transition from evaporative desorption to bulk ablation. This will be possible when moleular dynamics is used instead of the molecular beam approximation for the desorption event.

Magnitude of the Ion Yield

At a comfortably above-threshold fluence of 20 mJ/cm^2, the depth integrated ion yield predicted by the simulation is about 3 X10^{-4}, depending slightly on pulse length. This corresponds well with the experimentally measured values.(13, 29, 35) The yield increases significantly at higher fluences, also as experimentally observed.(13) As expected, the majority of the ions are generated in and released from layers near the surface. The main ionization mechanism at these fluences is $S_1 + S_n$ pooling.

Plume Temperatures

The peak temperatures reached for 20 mJ/cm^2 355 nm laser pulses are 525-550 K (calculated for the surface layer). These are again in good agreement with measured values of the plume temperature.(13, 35) The relatively low temperatures make thermal ionization from the S_n state quite inefficient, given the measured ionization potentials (IPs) for DHB and its larger clusters.(16, 17) Should the IPs drop substantially at larger sizes, or if shorter excitation wavelengths are used, this mechanism could also become more important. However, since thermal ionization depends exponentially on the energy gap from the higher excited state to the ion, this mechanism will only be significant when the gap becomes very small.

Plume Expansion Characteristics

In the molecular beam model of the plume, the expansion continues until the background pressure in the vacuum system is reached, so the velocity continues to increase asymptotically as well. However, the major part of the acceleration occurs during the first 5 ns after the start of desorption, and decreases steadily after that. After a typical simulation of 30-40 ns, the plume velocity has therefore reached values that can be meaningfully compared with experiment.

The surface layers were found to expand with a final speed of about 1200 m/s, in agreement with experiment. Although average DHB speeds are 500-600 m/s,(36) the fastest (surface) material moves about twice as quickly.(28, 37) Subsurface layers

are progressively slower, in agreement with the observation that ion velocities cover a significant range.(28, 37, 38) These results also correspond well with molecular dynamics calculations.(39)

Spot Size Effect

The MALDI ion yield depends not only on the laser fluence but also on the size of the irradiated sample spot.(13, 40) A complete explanation for this effect has been missing until now. The present model is capable of reproducing the major features of the spot size effect, as seen in Fig. 10. In part A is shown the ion yield for different spot sizes. It differs because the plume expansion is slower for larger spots, allowing fewer ions to form and escape. This yield is normalized to the irradiated sample volume. Compared on the basis of the illuminated area, the data have a different appearance, as shown in part B. More ions are created by larger laser spots, although the fractional yield is lower. Notable is the large difference between a small spot and the larger ones. This non-linear size dependence is as experimentally observed, as is the rightward rounded shape of the curves.(13, 40) Also, the apparent ion generation threshold has the same dependence as found experimentally.(13, 40) At the absolute yield corresponding to the smallest instrumentally detectable signal, is is clear from part B of the figure that the smaller spot will appear to have a higher threshold fluence.

Conclusions

The continuum rate equation model for UV-MALDI with DHB matrix is extended to include the effects of desorption. The plume is treated as an adiabatic, supersonic expansion, and the effect of the large entrained cluster content is included. This model is found to reproduce a range of experimental data with only minimal adjustment of a few parameters. Most of the parameters were fixed from experimental results for DHB or by analogy to known processes in other molecules. All model parameters lie well within physically reasonable bounds.

The most important results reproduced by the model (with a single parameter set) are the fluence dependence of the fluorescence yield (nanosecond pulses) and the shape of the picosecond delayed 2-pulse ion yield. The former is reproduced very well; the latter is reproduced in a semi-quantitative manner.

In addition, the model correctly:

- predicts the existence of a fluence threshold, in the correct fluence range. The threshold is determined by desorption, not ionization.
- predicts a fluence rather than irradiance dependence of the threshold, and a weak irradiance dependence above threshold
- predicts the laser wavelength dependence of the threshold
- predicts the existence of a 2-pulse effect for sub-threshold pulses
- predicts the magnitude of the ion yield
- predicts plume temperatures
- predicts plume expansion velocities
- predicts the spot size effect

The wide-ranging success of this model suggests that it substantially reflects the major processes active in DHB matrix under UV laser irradiation. MALDI is seen to be a fascinating interplay between the photochemical processes of ionization and the physical processes of desorption. Further refinement of the model appears to be most necessary for the desorption aspect. Combination of the ionization model presented here and a molecular dynamics approach to the plume is expected to be very fruitful and is in progress.

Acknowlegments

The author thanks H. Lüdemann for providing the fluorescence intensity data in digital form.

This work was supported by the Schweizerische Nationalfonds, Grant nr. 21-63558

Literature Cited

1. Knochenmuss R., Stortelder A., Breuker K. and Zenobi R. J. Mass Spectrom. 2000; 35: 1237.
2. Zenobi R. and Knochenmuss R. Mass Spectrom. Rev. 1998; 17: 337.
3. Knochenmuss R. and Zenobi R. Chem. Rev. 2002; submitted:
4. Karas M., Glückmann M. and Schäfer J. J. Mass Spectrom. 2000; 35: 1.
5. Knochenmuss R., Dubois F., Dale M. J. and Zenobi R. Rapid Commun. Mass Spectrom. 1996; 10: 871.
6. Tang X., Sadeghi M., Olumee Z. and Vertes A. Rapid Commun. Mass Spectrom. 1997; 11: 484.
7. Knochenmuss R. and Vertes A. J. Phys. Chem. B 2000; 104: 5406.
8. Chevrier M. R. and Cotter R. J. Rapid Commun. Mass Spectrom. 1991; 5: 611
9. Beavis R. C. Org. Mass Spectrom. 1992; 27: 864.
10. Demirev P., Westman A., Reimann C. T., Håkansson P., Barofsky D., Sundqvist B. U. R., Cheng Y. D., Seibt W. and K S. Rapid Commun. Mass Spectrom. 1992; 6: 187
11. Johnson R. E. Int. J. Mass Spectrom. Ion Proc. 1994; 139: 25.
12. Riahi K., Bolbach G., Brunot A., Breton F., Spiro M. and Blais J.-C. Rapid Commun. Mass Spectrom. 1994; 8: 242.
13. Dreisewerd K., Schürenberg M., Karas M. and Hillenkamp F. Int. J. Mass Spectrom. Ion Proc. 1995; 141: 127.
14. Dreisewerd K., Schürenberg M., Karas M. and Hillenkamp F. Int. J. Mass Spectrom. Ion Proc. 1996; 154: 171.
15. Ehring H., Karas M. and Hillenkamp F. Org. Mass Spectrom. 1992; 27: 427.
16. Karbach V. and Knochenmuss R. Rapid Commun. Mass Spectrom. 1998; 12: 968.
17. Lin Q. and Knochenmuss R. Rapid Comm. Mass Spectrom. 2001; 15: 1422.
18. Allwood D. A., Dyer P. E., Dreyfus R. W. and Perera I. K. Appl. Surf. Sci. 1997; 110: 616.
19. Allwood D. A., Dyer P. E. and Dreyfus R. W. Rapid Commun. Mass Spectrom. 1997; 11: 499.
20. Lüdemann H.-C., Redmond R. W. and Hillenkamp F. 2000 American Society of Mass Spectrometry, Long Beach, CA, 2000.
21. Yingling Y. G., Zhigilei L. V., Garrison B. J., Koubenakis A., Labrakis J. and Georgiou S. Appl. Phys. Lett. 2001; 78: 1631.
22. Zhigilei L. V. and Garrison B. J. Appl. Phys. Lett. 1999; 74: 1341.
23. Zhigilei L. V. and Garrison B. J. Appl. Phys. A 1999; 69: S75.
24. Zhigilei L. V., Kodali P. B. S. and Garrison B. J. Chem. Phys. Lett. 1997; 276: 269.

25. Breuker K., Knochenmuss R. and Zenobi R. Int. J. Mass Spectrom. 1999; 184: 25.
26. Stevenson E., Breuker K. and Zenobi R. J. Mass Spectrom. 2000; 35: 1035.
27. Miller D. R. Atomic and Molecular Beam Methods, G. Scoles (eds.). Oxford University Press: Oxford, 1988; 14.
28. Puretzky A. A., Geohegan D. B., Hurst G. B. and Buchanan M. V. Phys. Rev. Lett. 1999; 83: 444.
29. Puretzky A. A. and Geohegan D. B. Chem. Phys. Lett. 1997; 286: 425.
30. Handschuh M., Nettesheim S. and Zenobi R. Appl. Surf. Sci. 1998; 137: 125.
31. Birks J. B. Photophysics of Aromatic Compounds, Wiley Interscience: London, 1970.
32. Frankevich E., Ishii H., Hamanaka Y., Yokoyama T., Fuji A., Li S., Yoshino K., Nakamura A. and Seki K. Phys. Rev. B 2000; 62: 2505.
33. Karas M., Bachmann D. and Hillenkamp F. Anal. Chem. 1985; 57: 2935.
34. Heise T. W. and Yeung E. S. Anal. Chim. Acta 1995; 199: 377
35. Mowry C. D. and Johnston M. V. J. Phys. Chem. 1994; 98: 1904.
36. Glückmann M. and Karas M. J. Mass Spectrom. 1999; 34: 467.
37. Bökelmann V., Spengler B. and Kaufmann R. Eur. Mass Spectrom. 1995; 1: 81.
38. Kinsel G. R., Edmondson R. D. and Russell D. H. J. Mass Spectrom. 1997; 32: 714.
39. Zhigilei L. V. and Garrison B. J. Rapid Comm. Mass Spectrom. 1998; 12: 1273.
40. Feldhaus D., Menzel C., Berkenkamp S. and Hillenkamp F. J. Mass Spectrom. 2000; 35: 1320.

Table 1. Parameters used in simulation of DHB laser desorption / ionization at 355 nm.

IP (free molecule)	8.05 eV	Ref. 15
IP (large clusters)	7.82 eV	Ref. 16
S_1 state energy	3.466 eV	Ref. 15
starting temperature	298 K	
σ_{01}= $S_0 \rightarrow S_1$ absorption coeff.	9.9 X10^{-18} cm^2	Ref. 19
σ_{10}= $S_0 \leftarrow S_1$ stimulated emission	2 X10^{-18} cm^2	(1/5 of $S_0 \rightarrow S_1$)
σ_{1n}= $S_1 \rightarrow S_n$ absorption coeff.	2 X10^{-18} cm^2	(1/5 of $S_0 \rightarrow S_1$)
k_{n1}= $S_1 \leftarrow S_n$ decay rate	7.5 X10^{10} s^{-1}	(13 ps)
$t_1(t=0)$= solid state S_1 lifetime	1 ns	Ref. 19
t_1'= limiting plume S_1 lifetime	3 ns	(1/10 of measured gas phase)
$\Phi(t)$= fluorescence quantum yield	$t_1(t)/t_1$'	
f= internal degrees of freedom	45	(normal modes)
γ= Cp/Cv for plume expansion	1.05	(from degrees of freedom)
density	1.44 g/cm^3	
k_{I0} = Ion recombination	1.5 X10^{11} s^{-1}	(6.7 ps)
Fraction clusters in plume	0.85	Ref. 21,22
laser spot diameter	0.1 mm	
Pooling rate constants:		
k_{I1} = $S_1 + S_1 \rightarrow S_n + S_0$	7 X10^9 s^{-1}	(140 ps)
k_{In} = $S_1 + S_n \rightarrow$ Ions + S_0	1 X 10^{11} s^{-1}	(10 ps)
D= expansion scaling factor	P/P_0	

Figures

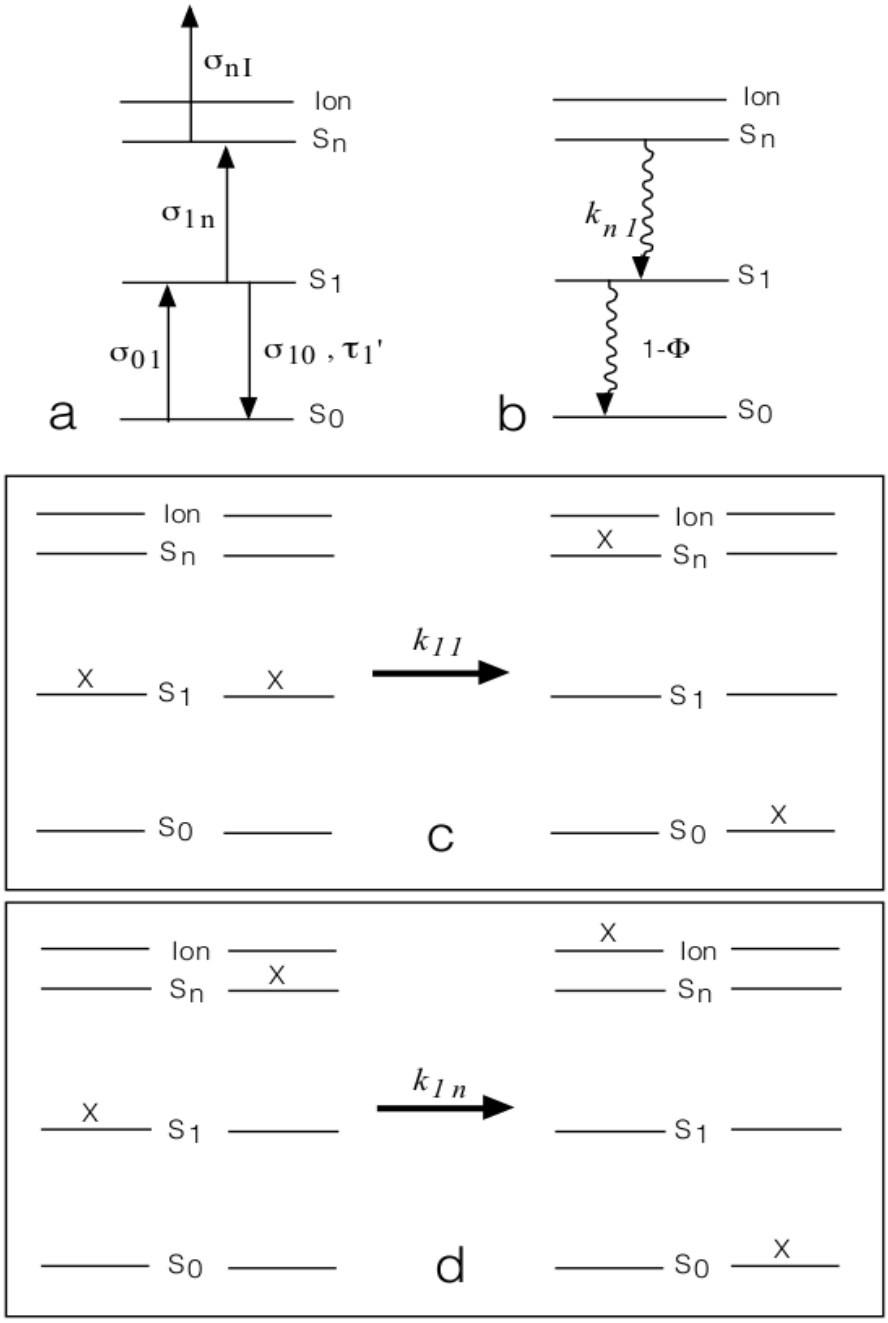

Figure 1. Schematic illustration of the states and processes modelled. a): Unimolecular radiative processes. Each arrow represents a separate laser-induced process. The downward step from S_1 to S_0 is not only stimulated by the laser but also occurs spontaneously (fluorescence). b): Non-radiative processes which convert electronic excitation into heat. c): Pooling of two S_1 excitations, yielding an isoenergetic system consisting of a S_n + ground state pair. d): Pooling of one S_1 and one S_n excitation, yielding a system consisting of an ion + ground state pair. The excess energy above the ion state is converted to heat. Not shown: recombination of an ion (with an electron or negative ion) to yield a ground state neutral.

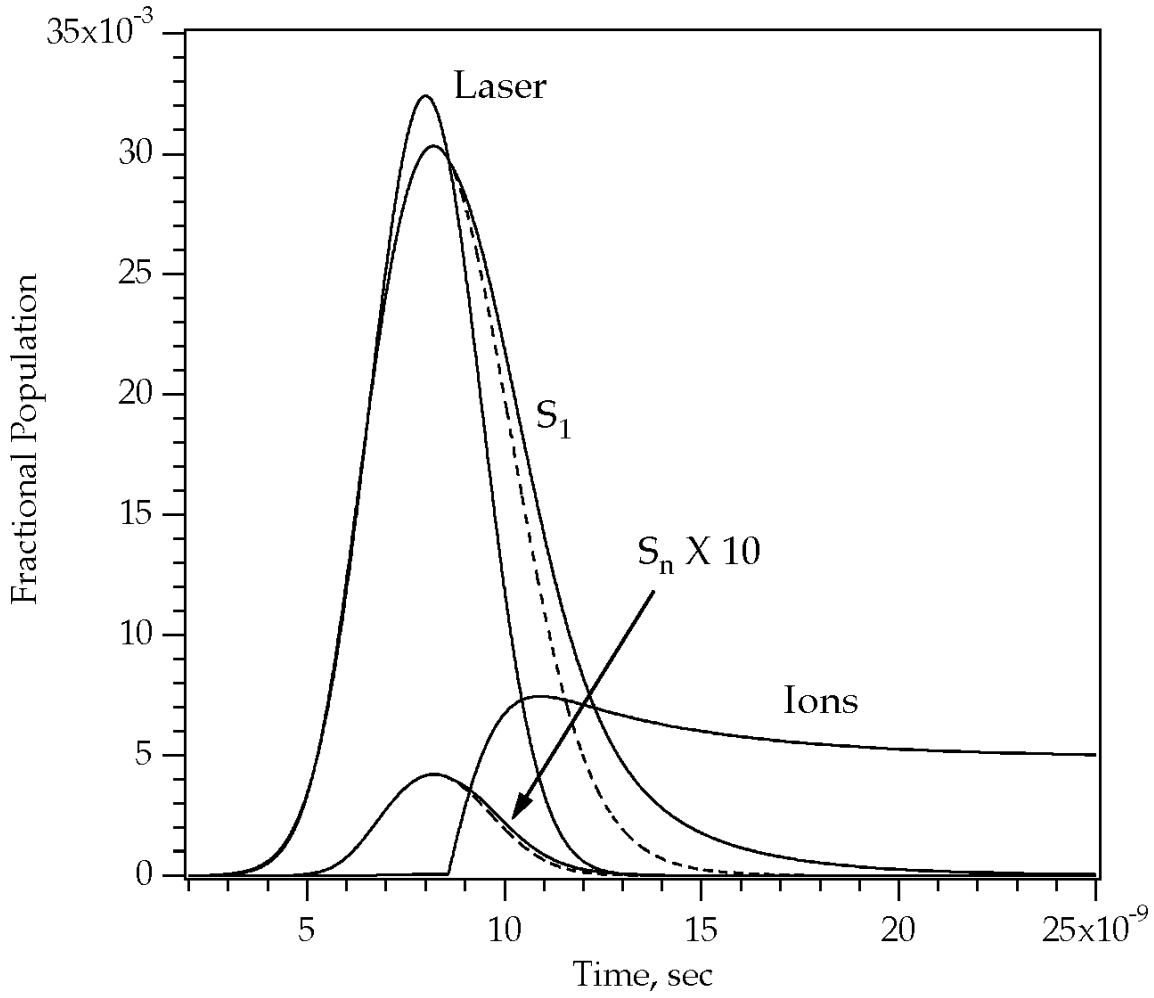

Figure 2. Simulated S_1, S_n and ion populations for a nanosecond 355 nm laser pulse in DHB matrix (20 mJ/cm^2). The parameters were as in Table 1. The solid lines are for "free" DHB that desorbs in molecular form. The dashed lines are for "solid" DHB clusters.

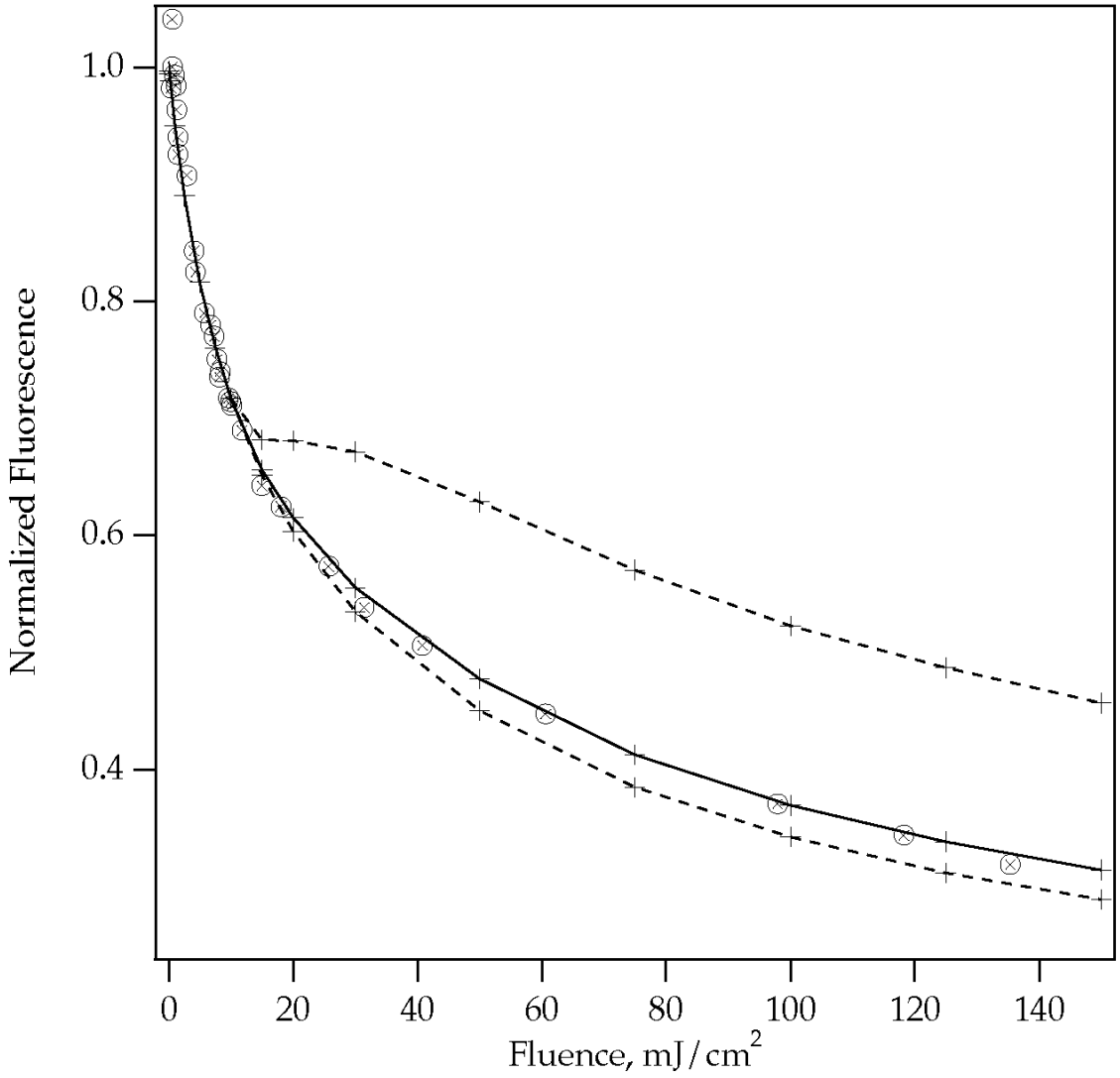
Normalized Fluorescence
1.0
0.8
0.6
0.4
0
20
40
60
80
100
120
140
Fluence, mJ/cm2

Fig 3a

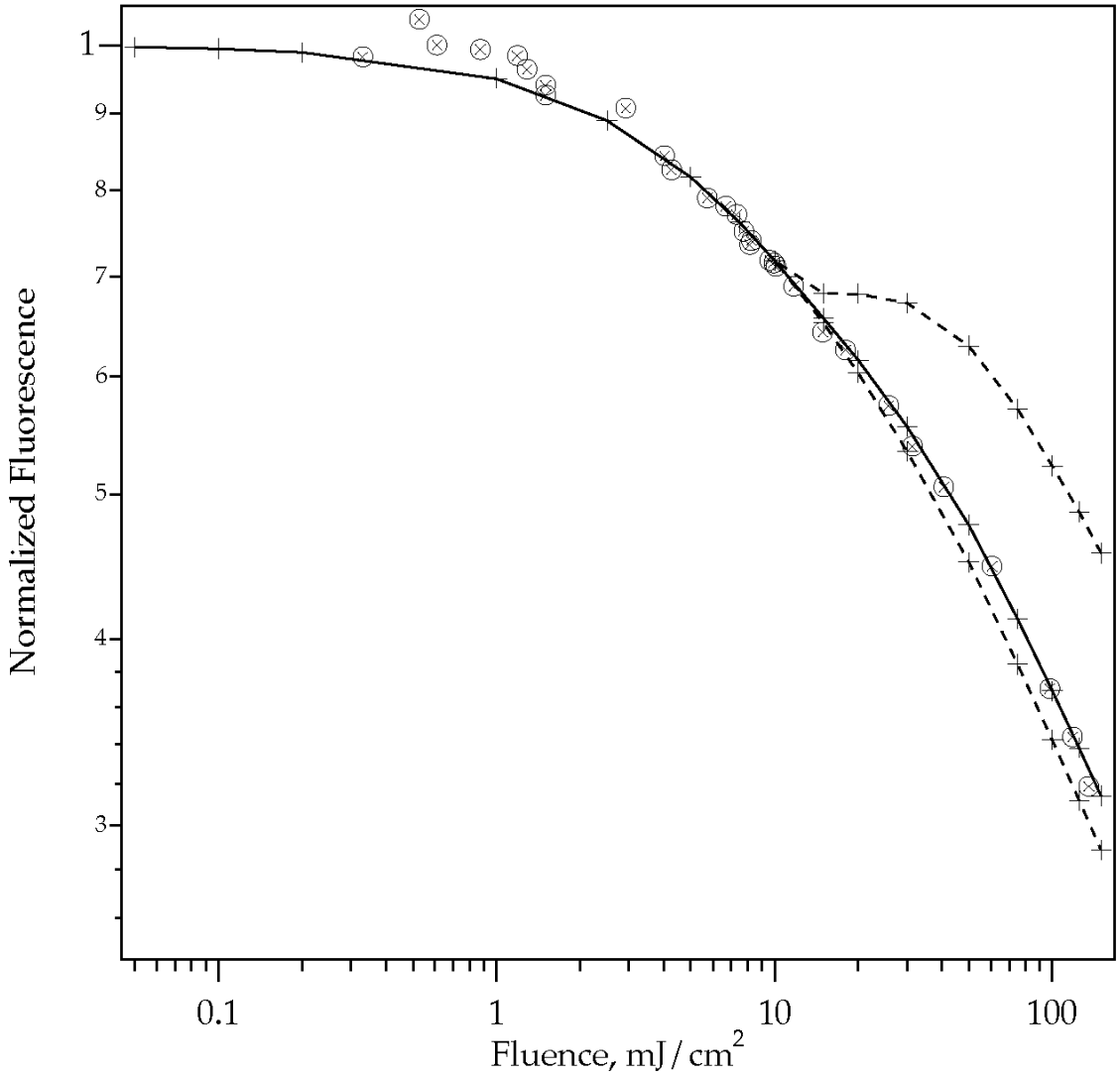

Fig 3b

Figure 3. Fluence dependence of the normalized fluorescence yield (fluorescence/fluence) for a DHB sample irradiated by 4.3 ns 355 nm laser pulse. The upper dashed line is the fluorescence yield from the "free" desorbing matrix, the lower dashed line is from the "clusters." These two components are combined to make the solid curve in a 15:85 ratio. Part (a): linear-linear plot, emphasizing the higher fluence range. Part (b): log-log plot emphasizing the lower fluence range. The solid curve is in excellent agreement with experimental data of Lüdemann, et al(20).

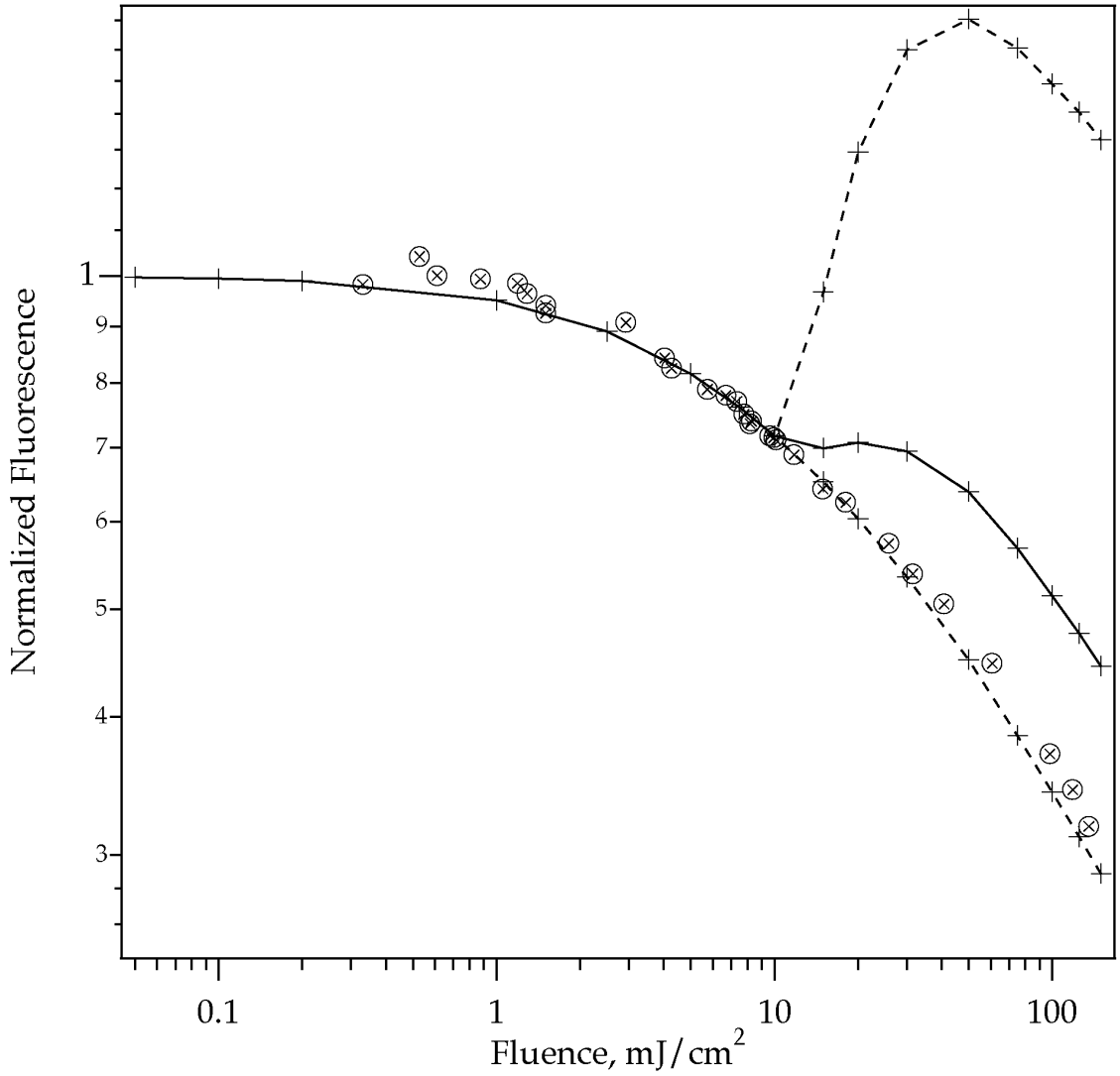
Normalized Fluorescence
1
9
8
7
6
5
4
3
0.1
1
10
100
Fluence, mJ/cm2

Fig 4a

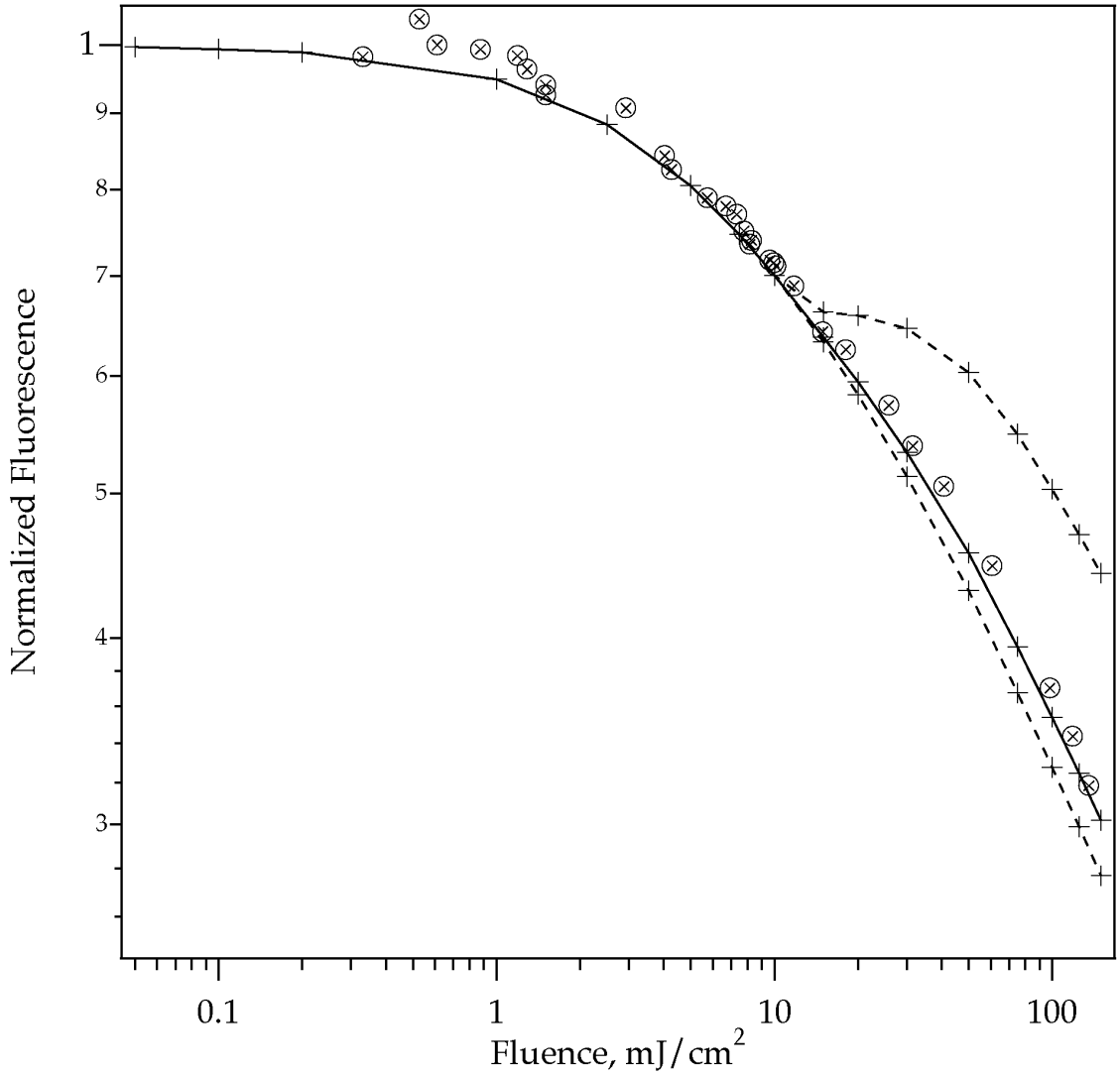

Fig4b

Figure 4. Fluence dependence of the normalized fluorescence yield as in Fig. 3, but with different model parameters. (a) The S_1 limiting plume lifetime has been increased from 3 ns to 10 ns. This has a large effect on the curves, the model is well constrained by the data. (b) The $S_1 + S_n$ pooling rate has been doubled to 3 X 10^{11} /s. Since this mostly affects ionization, the curves are only slightly different.

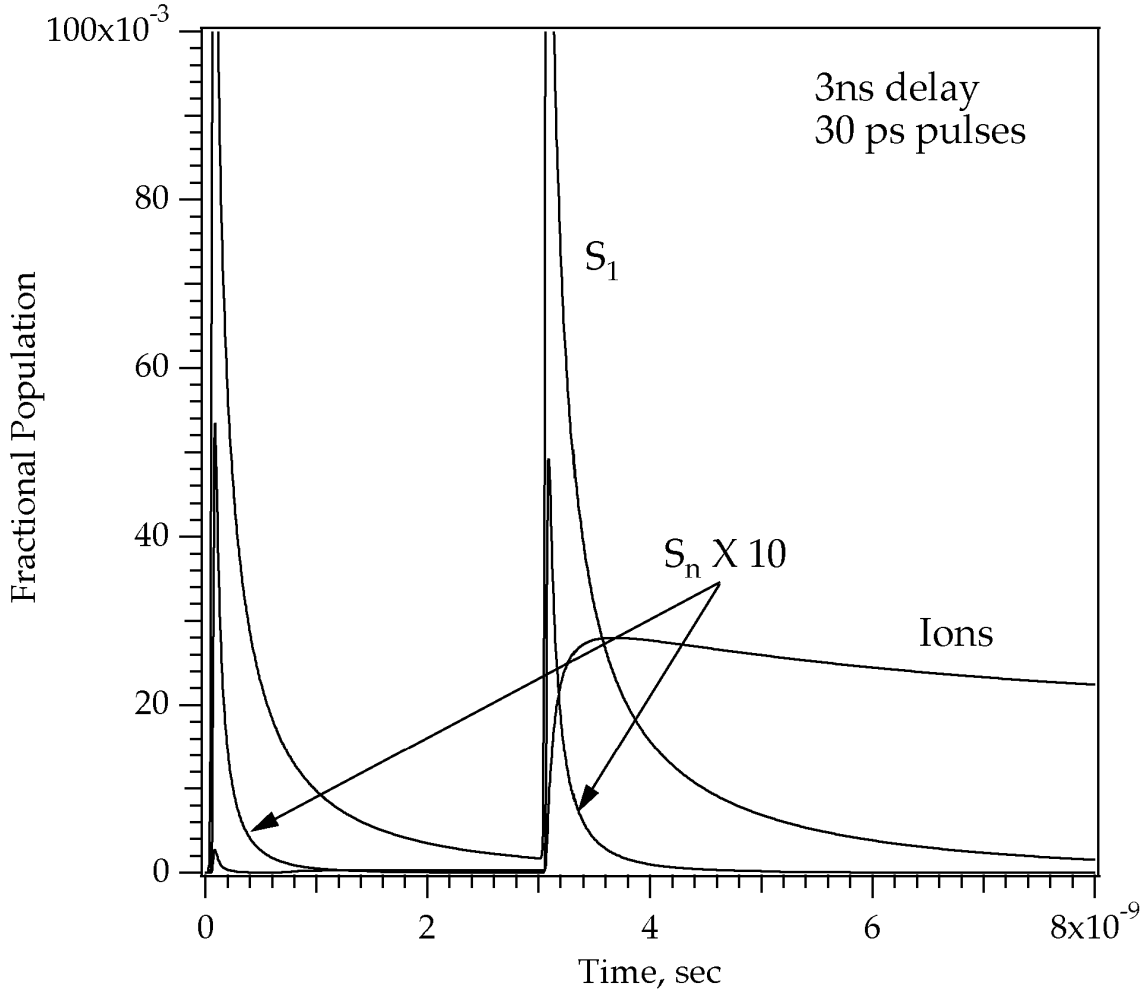

Figure 5. Simulated S_1, S_n and ion populations for two 30 picosecond 355 nm laser pulse in DHB matrix (13 mJ/cm^2). The parameters were as in Table 1. The solid lines are for "free" DHB that desorbs in molecular form. The dashed lines are for "solid" DHB clusters. The individual pulses are sub-threshold (few ions are generated, and they recombine), as seen for the first pulse. Because the first pulse heats the sample enough to start desorption, the second pulse is able to efficiently generate ions.

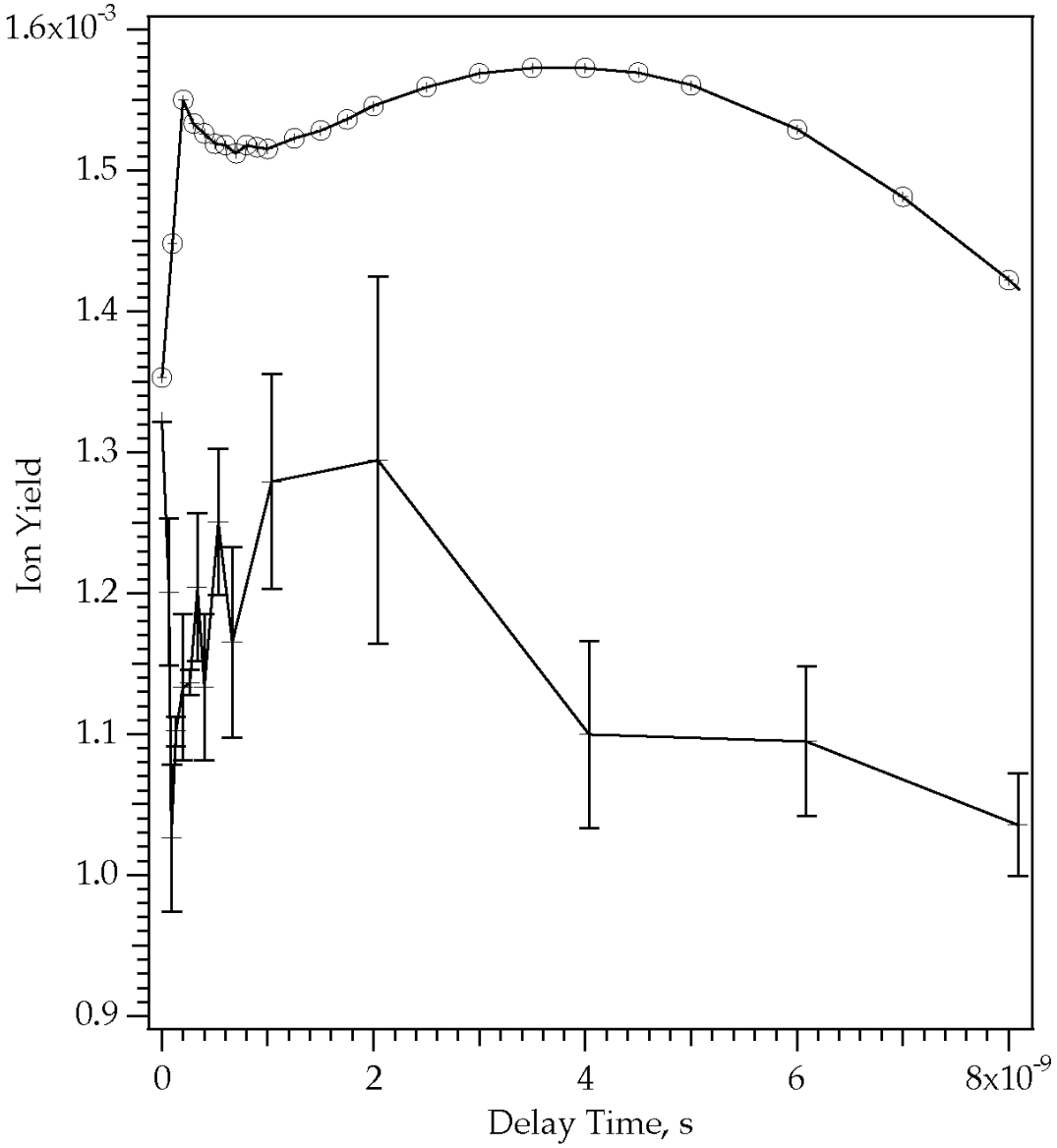

Fig 6a

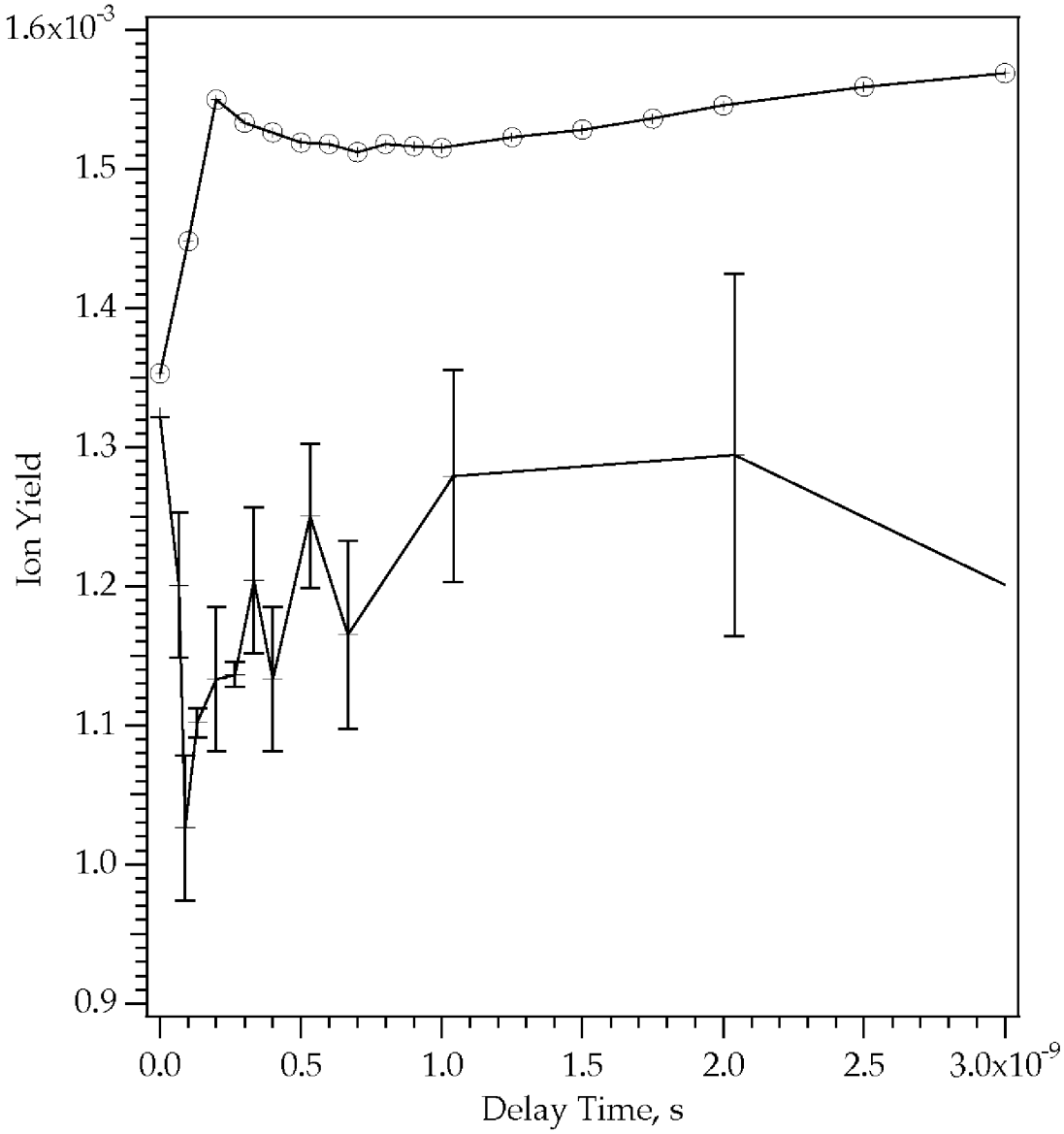

Fig 6b

Figure 6. Picosecond 2-pulse ion yield for two 15 mJ/cm^2 30 ps 355 nm laser pulses in DHB, as a function of delay between the pulses. The experimental data from Ref. (7) have been scaled for comparision. Part (a): broad delay time range. Part (b): the short time range, enabling comparison of the shape of the minima in the experimental and simulated curves.

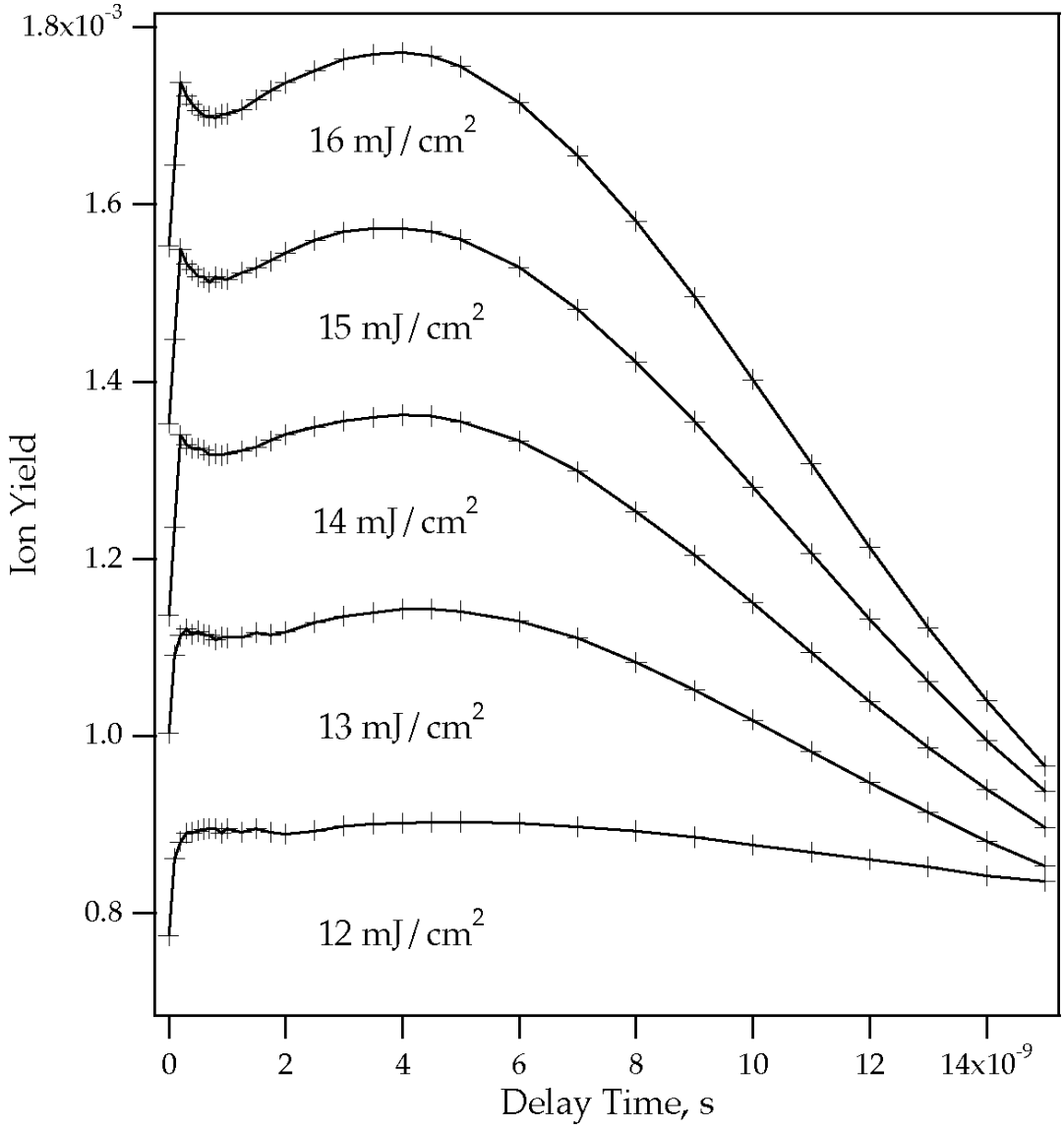

Figure 7. Dependence of the 2-pulse signal on fluence, using the parameters of Table 1. At the lowest fluence shown, desorption is induced only by the second pulse, giving a nearly constant ion yield. As the laser pulse energy is increased, desorption begins at earlier times, after the first pulse but before the second. This leads to the characteristic double-peaked delay time dependence.

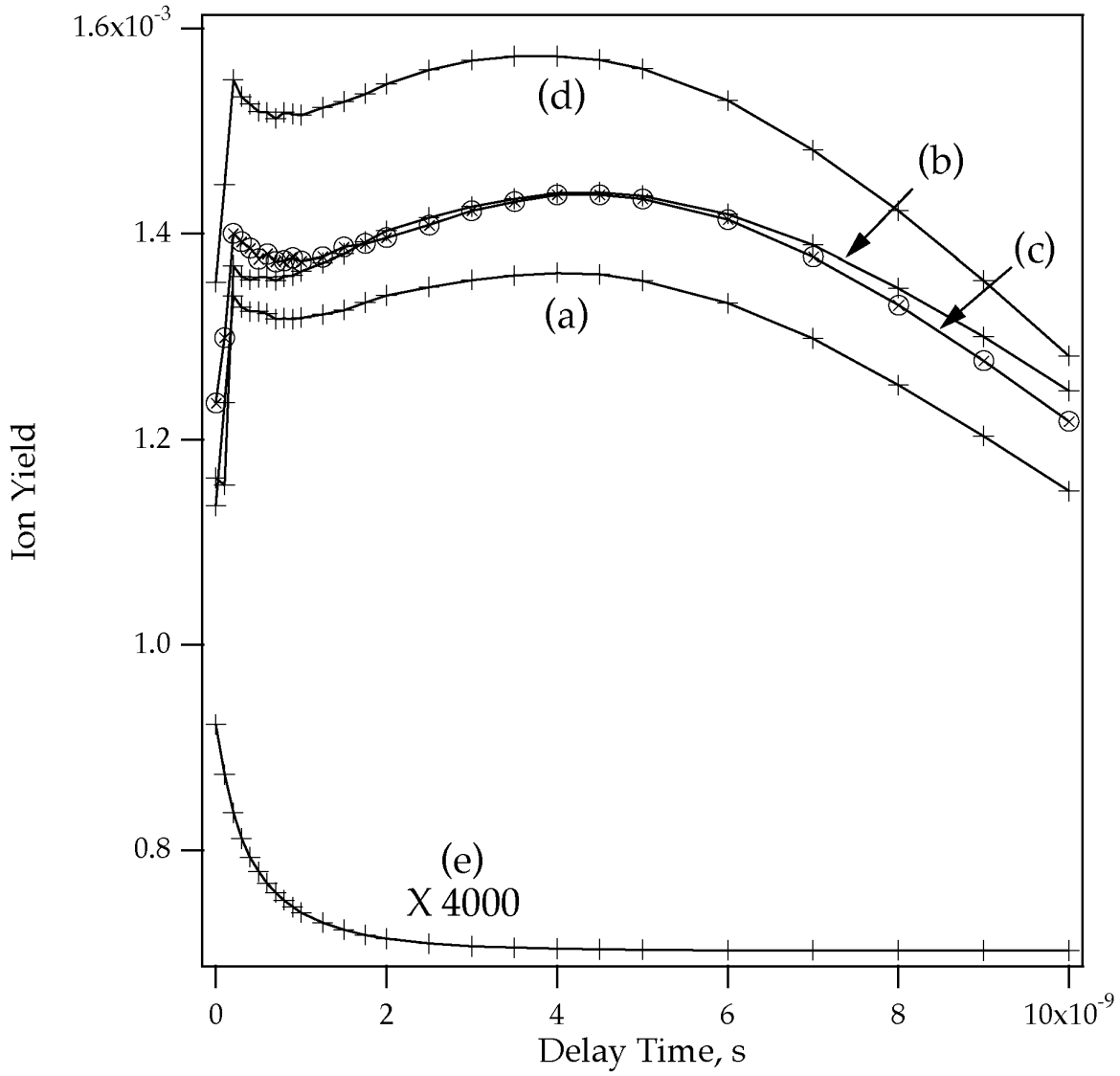

Figure 8. Dependence of the 2-pulse signal on model parameters. Curve (a) is for 14 mJ/cm^2, with the standard paramters (see also Fig. 6). For curve (b) the S1 limiting lifetime was increased from 3 ns to 10 ns. Curve (c) adds direct photoionization from the Sn state, with a cross section of 1X10^{-18} cm^2. In curve (d) the S_1 + S_n pooling rate was doubled to 3X10^{11} / s. Curve (e) is without plume expansion, and without ion recombination. The shape of the curve is incompatible with the data.

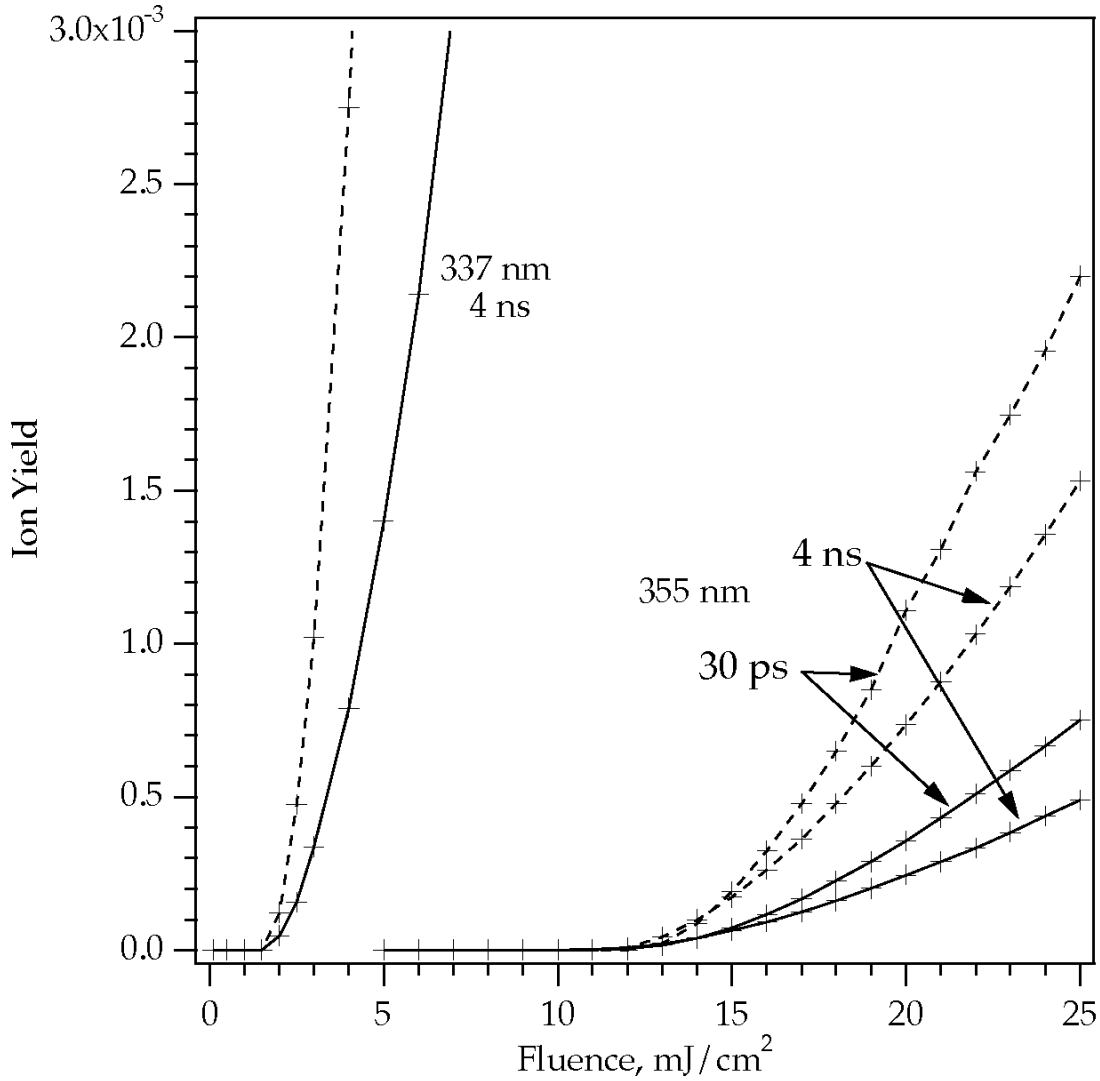

Figure 9. Ion yield vs. laser fluence in DHB matrix at two laser wavelengths. For 355 nm, two different pulse widths are shown. The open symbols are for simulations of the surface layer only. The closed symbols are depth-integrated. The threshold is the same for both 355 nm pulse widths, but the short pulse is somewhat more efficient at fluences above threshold. Because of the better absorption and higher photon energy, the 337 nm threshold is significantly lower.

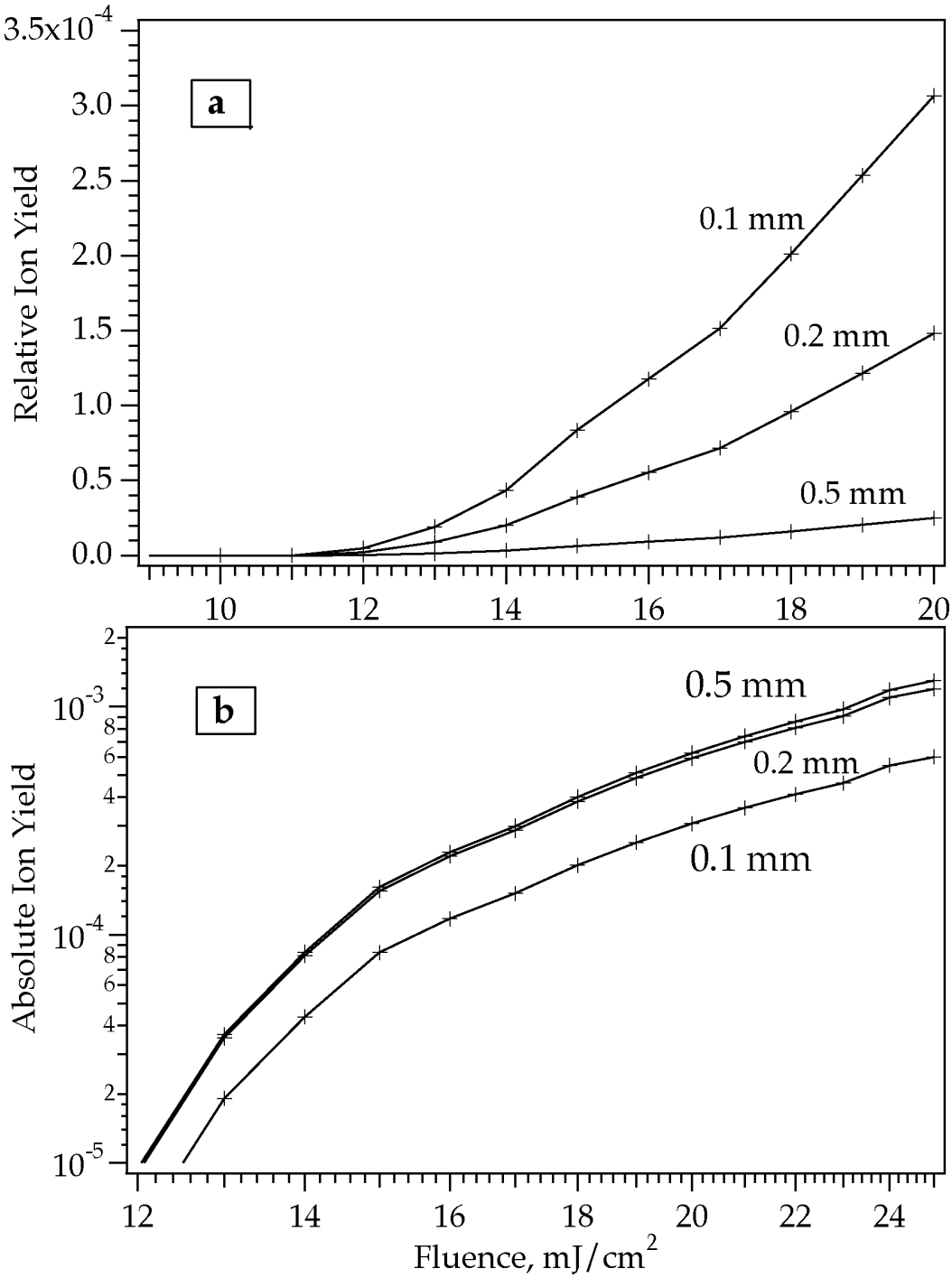

Figure 10. Ion yield vs. laser spot size, at 355 nm in DHB. In part A, the yield is shown relative to the irradiated volume. Smaller spots are seen to be more efficient in this sense. In part B, the data of part A are corrected for the relative areas of the spots. The larger spots yield more total ions, although with lower efficiency. The non-linear trend in yield vs. spot size is as observed experimentally (see text).